



Exact magnetic properties for classical delta-chains with ferromagnetic and antiferromagnetic interactions in applied magnetic field

D. V. Dmitriev  and V. Ya. Krivnov **Institute of Biochemical Physics of RAS, Kosygin Strasse 4, 119334 Moscow, Russia*

J. Schnack

Fakultät für Physik, Universität Bielefeld, Postfach 100131, D-33501 Bielefeld, Germany

J. Richter

*Institut für Physik, Otto-von-Guericke-Universität Magdeburg, P.O. Box 4120, 39016 Magdeburg, Germany
and Max-Planck-Institut für Physik komplexer Systeme, Nöthnitzer Straße 38, 01187 Dresden, Germany*

(Received 11 November 2019; revised manuscript received 9 January 2020; accepted 5 February 2020; published 19 February 2020)

We study the thermodynamics of the delta-chain with competing ferro- and antiferromagnetic interactions in an external magnetic field which generalizes the field-free case studied previously. This model plays an important role for the recently synthesized compound $\text{Fe}_{10}\text{Gd}_{10}$, which is nearly quantum critical, as well as for the new kagome fluoride $\text{Cs}_2\text{LiTi}_3\text{F}_{12}$. The classical version of the model is solved exactly and explicit analytical results for the low-temperature thermodynamics are obtained. The s -spin quantum model is studied using exact diagonalization and finite-temperature Lanczos techniques. Particular attention is focused on the magnetization and the susceptibility. The magnetization of the classical model in the ferromagnetic part of the phase diagram defines the universal scaling function which is valid for the quantum model. The dependence of the susceptibility on the spin quantum number s at the critical point between the ferro- and ferrimagnetic phases is studied and the relation to $\text{Fe}_{10}\text{Gd}_{10}$ is discussed.

DOI: [10.1103/PhysRevB.101.054427](https://doi.org/10.1103/PhysRevB.101.054427)

I. INTRODUCTION

Low-dimensional quantum magnets on geometrically frustrated lattices have been extensively studied in recent years [1–3]. One of the interesting classes of such systems includes lattices consisting of triangles. A typical example of these objects is the delta or the sawtooth chain, i.e., a Heisenberg model defined on a linear chain of triangles, as shown in Fig. 1. The Hamiltonian of this model has the form

$$\hat{H} = J_1 \sum \sigma_i \cdot (\mathbf{S}_i + \mathbf{S}_{i+1}) + J_2 \sum \mathbf{S}_i \cdot \mathbf{S}_{i+1} - H \sum (\sigma_i^z + S_i^z), \quad (1)$$

where σ_i and S_i are the apical and the basal spins, correspondingly, H is the external magnetic field, and J_1 and J_2 are apical-basal and basal-basal interactions. A direct interaction between the apical spins is absent.

The quantum $s = \frac{1}{2}$ delta-chain with antiferromagnetic (AF) exchange interactions J_1 and J_2 ($J_1, J_2 > 0$) has been studied extensively and it exhibits a variety of peculiar properties [4–10]. At the same time, the $s = \frac{1}{2}$ delta-chain with ferromagnetic J_1 and antiferromagnetic J_2 interaction (F-AF delta-chain) is very interesting as well and has unusual properties depending on the frustration parameter $\alpha = \frac{J_2}{|J_1|}$ [11–14]. In particular, the ground state of this model is ferromagnetic for $\alpha < \frac{1}{2}$ and it is believed [11] that it is ferrimagnetic for

$\alpha > \frac{1}{2}$. The critical point $\alpha = \frac{1}{2}$ is the transition point between these two ground-state phases. The ground-state properties of the model in this point are highly nontrivial. For example, the $s = \frac{1}{2}$ F-AF delta-chain studied in Ref. [13] has a class of localized magnon bound states which form a macroscopically degenerate ground-state manifold hosting already half of the maximum total entropy $N \ln 2$. The $s = \frac{1}{2}$ F-AF delta-chain is a minimal model for a description of real compounds, in particular malonate-bridged copper complexes [11,12,15,16], as well as the new kagome fluoride $\text{Cs}_2\text{LiTi}_3\text{F}_{12}$, which, besides spin chains, hosts delta-chains as magnetic subsystems [17].

The $s = \frac{1}{2}$ F-AF model can be extended to the delta-chain composed of two types of spins (σ_i, \mathbf{S}_i) characterized by the spin quantum numbers S_a and S_b of the apical and basal spins, respectively. The ground state of this model is ferromagnetic (F) for $\alpha < \alpha_c$ and noncollinear ferrimagnetic for $\alpha > \alpha_c$, where $\alpha_c = S_a/2S_b$. For $S_a = S_b$, the critical point is at $\alpha_c = \frac{1}{2}$. The ground state of the model with any quantum numbers S_a and S_b in the critical point α_c consists of the exact same multimagnon states as for the $s = \frac{1}{2}$ model and has similar macroscopic degeneracy [13].

An additional motivation for the study of the (S_a, S_b) F-AF delta-chain is the existence of a recently synthesized mixed $3d/4f$ cyclic coordination cluster, $[\text{Fe}_{10}\text{Gd}_{10}(\text{Me-tea})_{10}(\text{Me-teaH})_{10}(\text{NO}_3)_{10}]20\text{MeCN}$ (i.e., $\text{Fe}_{10}\text{Gd}_{10}$) [18,19], with the ground-state spin $S = 60$. This cluster consists of 10 + 10 alternating gadolinium ($S = \frac{7}{2}$)

*krivnov@deom.chph.ras.ru

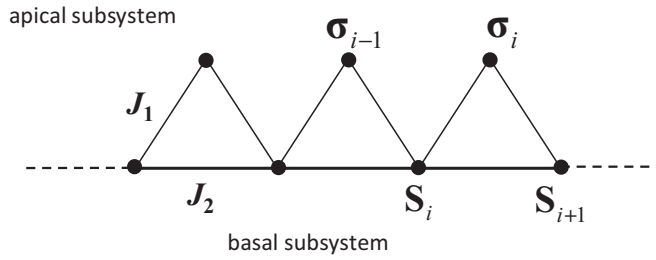


FIG. 1. The delta-chain model.

and iron ($S = \frac{5}{2}$) ions and its spin arrangement corresponds to the delta-chain with Gd and Fe ions as the apical and basal spins, correspondingly. This molecule is a finite-size realization of the F-AF delta-chain with $J_1 = -2.0$ and $J_2 = 1.3$ K and $S_a = \frac{7}{2}$ and $S_b = \frac{5}{2}$. The frustration parameter $\alpha = 0.65$ is very close to the critical value $\alpha_c = 0.7$. Because the spin quantum numbers for Fe and Gd ions are rather large, it seems that the classical approximation for the (S_a, S_b) F-AF delta-chain is justified.

In our preceding work [20], we studied both classical and quantum versions of the F-AF delta-chain at zero magnetic field. It was shown that the classical model provides a reasonable description of the thermodynamics of $\text{Fe}_{10}\text{Gd}_{10}$ down to moderate temperatures and some properties of the quantum spin delta-chain are correctly described by the classical model. For example, the main features of the zero-field susceptibility χ of the quantum spin delta-chain are reproduced by the classical model.

However, the results of the paper [20] are related to the zero-field case. The experimental data for $\text{Fe}_{10}\text{Gd}_{10}$ presented in Ref. [18] demonstrate that there is a strong influence of a magnetic field on the low-temperature thermodynamics. That is related to the massively degenerate manifold of localized magnon states having different total magnetization. The Zeeman term will partly lift this degeneracy, and in this way influence the low-energy spectrum substantially. Therefore, it is interesting to consider the thermodynamic behavior of the classical delta-chain in a magnetic field. In this paper, we will study the classical delta-chain in the external magnetic field. This model is more complicated in comparison with that for $H = 0$. Nevertheless, it can be solved exactly and the analytical results for the low-temperature properties are explicitly obtained. We calculate the magnetization curve $M(H)$ and the susceptibility and compare them with the results for the quantum model. For example, we can quantitatively explain the experimental result related to a maximum of MT/H vs T for $\text{Fe}_{10}\text{Gd}_{10}$.

For simplicity and to avoid cumbersome formulas, we will consider the spin- s delta-chain, i.e., the model with $S_a = S_b = s$. (The extension of results for the case $S_a \neq S_b$ can be obtained straightforwardly.) We note that the frustration parameter $\alpha = 0.65$ for the $\text{Fe}_{10}\text{Gd}_{10}$ molecule with $S_a = \frac{7}{2}$, $S_b = \frac{5}{2}$ corresponds to $\alpha \simeq 0.45$ for the model with $S_a = S_b = 3$, and it is expected that the behavior of the two models for these frustration parameters is very similar. In accordance with the adopted simplification, we will further consider the F-AF delta-chain with $s = 3$ and $\alpha = 0.45$ as a model for the $\text{Fe}_{10}\text{Gd}_{10}$ molecule.

The paper is organized as follows. In Sec. II A, we describe the ground state of the classical model (2) in different regions of the frustration parameter α including the critical value $\alpha = \frac{1}{2}$. The partition function and the magnetization are calculated in Sec. II B. In Sec. II C, explicit analytical results in the low-temperature limit are presented for different regions of the parameter α and the scaling law for $\alpha \leq \frac{1}{2}$ is established. In Sec. III, the quantum effects at low temperatures will be studied by a combination of full exact diagonalization (ED) using Schulenburg's SPINPACK code [21] and the finite-temperature Lanczos (FTL) technique [22,23]. We compare the magnetization of the classical and the quantum models and estimate finite-size effects.

II. CLASSICAL SPIN Δ -CHAIN IN A MAGNETIC FIELD

To obtain the classical version of Hamiltonian (1), we set $\sigma_i = s\vec{n}_i$ and $S_i = s\vec{n}_i$, where \vec{n}_i is the unit vector at the i th site. Taking the limit of infinite s , we arrive at the Hamiltonian of the classical delta-chain,

$$\mathcal{H} = - \sum_{i=1}^N \vec{n}_i \cdot \vec{n}_{i+1} + \alpha \sum_{i=1}^{N/2} \vec{n}_{2i-1} \cdot \vec{n}_{2i+1} - h \sum_{i=1}^N n_i^z, \quad (2)$$

where N is the number of spins. In Eq. (2), we take the apical-basal interaction as -1 and the basal-basal interaction as α .

In this section, we use the normalized magnetic field and temperature,

$$h = H/s, \quad (3)$$

$$t = T/s^2, \quad (4)$$

and the corresponding inverse temperature $\beta = 1/t$ to present the thermodynamic properties of model (2).

A. Ground state

We start our study of model (2) from the determination of the ground state. For this aim, it is useful to represent Hamiltonian (2) as a sum over triangle Hamiltonians,

$$\mathcal{H} = \sum_{i=1}^{N/2} \mathcal{H}_{\Delta}(i), \quad (5)$$

where the Hamiltonian of the i th triangle has the form

$$\mathcal{H}_{\Delta}(i) = -\vec{n}_{2i-1} \cdot \vec{n}_{2i} - \vec{n}_{2i} \cdot \vec{n}_{2i+1} + \alpha \vec{n}_{2i-1} \cdot \vec{n}_{2i+1} - \vec{h} \cdot \left(\frac{1}{2} \vec{n}_{2i-1} + \vec{n}_{2i} + \frac{1}{2} \vec{n}_{2i+1} \right). \quad (6)$$

To determine the ground state of model (5), we need to find the spin configuration on each triangle which minimizes the classical energy. It turns out that the lowest spin configuration on a triangle is different in the regions $\alpha \leq \frac{1}{2}$ and $\alpha > \frac{1}{2}$. For $\alpha \leq \frac{1}{2}$, the ground state is the trivial ferromagnetic one with all spins on each triangle pointing in the same direction. The global spin configuration of the whole system in this case is obviously ferromagnetic as well.

For $\alpha > \frac{1}{2}$, the lowest classical energy on each triangle is given by a noncollinear ferrimagnetic configuration, where all spins of triangle $\vec{n}_1, \vec{n}_2, \vec{n}_3$ lie in the same plane and spin \vec{n}_2 assumes an equal angle θ_0 with spins \vec{n}_1 and \vec{n}_3 . The global

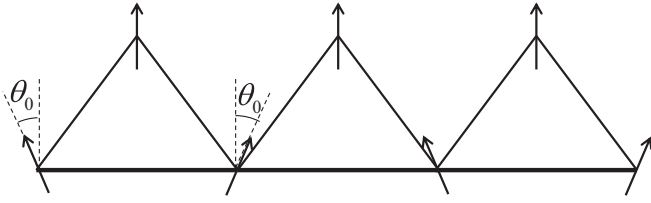


FIG. 2. The ferrimagnetic ground state of the classical delta-chain.

ground state without magnetic field of the whole system for $\alpha > \frac{1}{2}$ is macroscopically degenerate [24]. The magnetic field lifts this degeneracy and stabilizes the ferrimagnetic configuration where all apical spins are directed along the magnetic field and the basal spins are inclined by an equal angle θ_0 to the right and to the left of the field direction, as shown in Fig. 2. Therefore,

$$\vec{h} \cdot \vec{n}_2 = h, \quad (7)$$

$$\vec{n}_1 \cdot \vec{n}_2 = \vec{n}_2 \cdot \vec{n}_3 = \cos \theta_0, \quad (8)$$

$$\vec{n}_1 \cdot \vec{n}_3 = \cos(2\theta_0), \quad (9)$$

$$\cos \theta_0 = \frac{2+h}{4\alpha}. \quad (10)$$

The magnetization of the ground state in the ferrimagnetic region is

$$M_{gs} = \frac{2\alpha+1}{4\alpha} + \frac{h}{8\alpha} \quad (11)$$

for $h < h_{\text{sat}}$, where the saturated field in the ground state is defined by condition $\theta_0 = 0$:

$$h_{\text{sat}} = 4\alpha - 2. \quad (12)$$

B. Partition function

The partition function Z of model (2) is

$$Z = \left(\prod_{i=1}^N \int d\vec{n}_i \right) \exp(-\beta\mathcal{H}). \quad (13)$$

In our previous paper [20], we used local coordinate systems associated with the i th spin, which substantially simplified calculations. For the system in a magnetic field, this trick does not work. Therefore, we follow a common transfer-matrix method which reduces the calculation of the partition function in one-dimensional (1D) systems to an integral equation [25,26]. In our case, this integral equation is written for one triangle and has the form

$$\int e^{-\beta\mathcal{H}_\Delta(1)} \psi_i(\vec{n}_1) d\vec{n}_2 d\vec{n}_1 = \lambda_i \psi_i(\vec{n}_3). \quad (14)$$

The eigenvalues λ_i define the partition function as

$$Z = \sum \lambda_i^{N/2}. \quad (15)$$

In the thermodynamic limit $N \rightarrow \infty$, only the largest eigenvalue λ_0 survives,

$$Z \rightarrow \lambda_0^{N/2}. \quad (16)$$

Selecting the terms containing the apical spin \vec{n}_2 in the Hamiltonian of one triangle (6),

$$\mathcal{H}_\Delta(1) = -\vec{n}_2 \cdot (\vec{n}_1 + \vec{n}_3 + \vec{h}) + \alpha \vec{n}_1 \cdot \vec{n}_3 - \frac{1}{2} \vec{h} \cdot (\vec{n}_1 + \vec{n}_3), \quad (17)$$

we can explicitly integrate the integral equation (14) over the apical spin \vec{n}_2 ,

$$\int d\vec{n}_2 \exp[\beta \vec{n}_2 \cdot (\vec{n}_1 + \vec{n}_3 + \vec{h})] = \frac{\sinh(\beta h_a)}{\beta h_a}, \quad (18)$$

where h_a is the effective magnetic field acting on the apical spin \vec{n}_2 ,

$$h_a = \sqrt{(\vec{n}_1 + \vec{n}_3 + \vec{h})^2}. \quad (19)$$

Then, the integral equation (14) becomes

$$\int R(\vec{n}_1, \vec{n}_3) \psi_i(\vec{n}_1) d\vec{n}_1 = \lambda_i \psi_i(\vec{n}_3), \quad (20)$$

with the kernel depending on the basal spins only,

$$R(\vec{n}_1, \vec{n}_3) = \frac{\sinh(\beta h_a)}{\beta h_a} \exp \left[-\beta \alpha \vec{n}_1 \cdot \vec{n}_3 + \frac{1}{2} \beta \vec{h} \cdot (\vec{n}_1 + \vec{n}_3) \right]. \quad (21)$$

Equation (20) implies that the calculation of the thermodynamics of the delta-chain is reduced to the thermodynamics of the basal spin chain with a special form of interactions, which depend on the temperature.

Now we choose the coordinate system so that the magnetic field is directed along the Z axis. Then, $\vec{h} = (0, 0, h)$, and unit vectors \vec{n} have components $(\sin \theta \cos \varphi, \sin \theta \sin \varphi, \cos \theta)$, thus

$$\vec{n}_1 \cdot \vec{n}_3 = \cos \theta_1 \cos \theta_3 + \sin \theta_1 \sin \theta_3 \cos(\varphi_1 - \varphi_3), \quad (22)$$

and the effective magnetic field (19) is

$$h_a = \sqrt{2 + h^2 + 2\vec{n}_1 \cdot \vec{n}_3 + 2h(\cos \theta_1 + \cos \theta_3)}. \quad (23)$$

Now we notice that the kernel R in Eq. (21) contains the azimuthal angles φ_1, φ_3 only as a difference $(\varphi_1 - \varphi_3)$. Then we substitute, for the eigenfunctions,

$$\psi_i(\vec{n}_j) = e^{im\varphi_j} \phi_{m,i}(\theta_j), \quad (24)$$

and, in terms of $x_j = \cos \theta_j$, the integral equation (20) becomes

$$\int_{-1}^1 K_m(x_1, x_3) \phi_{m,i}(x_1) dx_1 = \lambda_{m,i} \phi_{m,i}(x_3), \quad (25)$$

with the symmetric kernel defined by an integral over $\varphi = (\varphi_1 - \varphi_3)$:

$$K_m(x_1, x_3) = \int_0^{2\pi} \frac{d\varphi}{4\pi} e^{im\varphi} R_{13}(\varphi, x_1, x_3). \quad (26)$$

The largest eigenvalue is always given by $m = 0$. The states with $m > 0$ become relevant in the calculations of transverse correlation functions [25], which we do not consider here. Therefore, below we put $m = 0$.

Thus, the thermodynamics of the delta-chain in the magnetic field (2) is reduced to the integral equation (25) over one variable, which can easily be calculated numerically. The numerical results of Eq. (25) will be discussed in the next sections.

C. Classical Δ -chain in a magnetic field at low temperature

In general, Eq. (25) completely describes the thermodynamics of the spin delta-chain in a magnetic field (2). However, in this section, we focus on the low-temperature limit, where explicit analytical results for the magnetization curve are possible.

At $t \rightarrow 0$, the integration in Eq. (20) can be carried out using the saddle-point method. For this aim, we need to expand the kernel R in Eq. (21) near its maximum. At first we notice that the effective magnetic field on the apical spin in the ground state is

$$\begin{aligned} h_{gs} &= 2 + h, & \alpha \leq \frac{1}{2}, \\ h_{gs} &= \frac{1}{\alpha} + \frac{1 + 2\alpha}{2\alpha}h, & \alpha > \frac{1}{2}. \end{aligned} \quad (27)$$

As follows from Eq. (27), h_{gs} is of the order of unity, except for the case $\alpha \rightarrow \infty$ and $h = 0$, which is not considered here. Therefore, in the low-temperature limit, $\beta h_a \gg 1$ and one can neglect the second term in $\sinh(\beta h_a)$. Similarly, the denominator in Eq. (21) can be substituted by its ground-state value, so that the kernel R in the saddle-point approach is approximated as

$$R \approx \frac{\exp(-\beta \mathcal{H}_{13})}{2\beta h_{gs}}, \quad (28)$$

where

$$\mathcal{H}_{13} = -h_a + \alpha \vec{n}_1 \cdot \vec{n}_3 - \frac{1}{2} \vec{h} \cdot (\vec{n}_1 + \vec{n}_3). \quad (29)$$

This implies that in the low- t limit, the behavior of the delta-chain system is described by the special form of the Hamiltonian acting on the basal chain only,

$$\begin{aligned} \mathcal{H}_{\text{eff}} &= - \sum \sqrt{2 + 2\vec{n}_{2i-1} \cdot \vec{n}_{2i+1} + 2h(n_{2i-1}^z + n_{2i+1}^z)} + h^2 \\ &+ \alpha \sum \vec{n}_{2i-1} \cdot \vec{n}_{2i+1} - h \sum n_{2i-1}^z. \end{aligned} \quad (30)$$

The integral equation (20) with the approximate expression for kernel (28) has the form

$$\int \frac{\exp(-\beta \mathcal{H}_{13})}{2\beta h_{gs}} \psi(\vec{n}_1) d\vec{n}_1 = \lambda \psi(\vec{n}_3). \quad (31)$$

The saddle point of Eq. (31) corresponds to the ground state of the local Hamiltonian H_{13} . Since the ground state of H_{13} is different in the regions $\alpha \leq \frac{1}{2}$ and $\alpha > \frac{1}{2}$, it is necessary to study these cases separately.

1. Ferromagnetic region and critical point $\alpha \leq \frac{1}{2}$

The low-temperature thermodynamics of the classical ferromagnetic chain ($\alpha = 0$) in the magnetic field was calculated in Ref. [27] by taking the continuum limit of the model. It was shown that the problem is mapped to the quantum rotator in the gravitational field $g = h/t^2$:

$$\left(\frac{1}{2} \hat{L}^2 - gn_z \right) \psi(\vec{n}) = \mu \psi(\vec{n}). \quad (32)$$

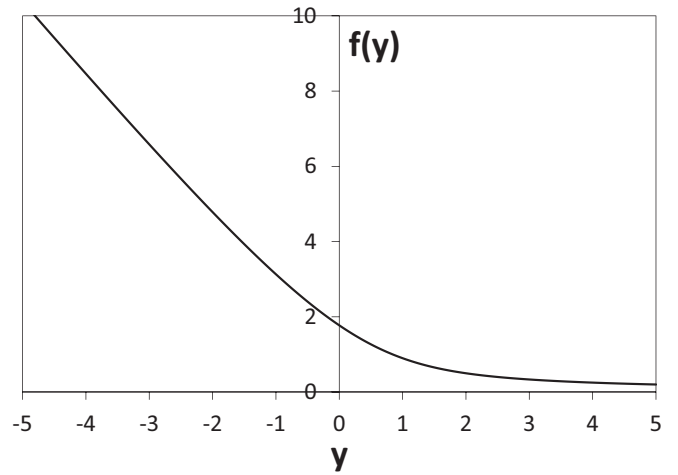


FIG. 3. Scaling function $f(y)$ given by Eq. (36).

The normalized magnetization is given by the scaling function $M(t, h) = \phi(g)$, where $\phi(g)$ is determined from the ground-state energy μ_0 of Eq. (32) by the relation [27]

$$\phi(g) = -\frac{d\mu_0}{dg}. \quad (33)$$

The expansion of the function $\phi(g)$ for small and large g as well as the numerical calculation of $\phi(g)$ were obtained in Ref. [27]. It was shown in Ref. [28] that the function $\phi(g)$ is well described by the approximate equation

$$g = \phi(g) - \frac{1}{4} + \frac{1}{4[1 - \phi(g)]^2}. \quad (34)$$

It turns out (see the Appendix) that the low-temperature thermodynamics of the classical delta-chain given by Eq. (2) is also described by the quantum rotator in the gravitational field, which has the specific form

$$g = \frac{h}{2t^{3/2}} f(y), \quad (35)$$

where

$$f(y) = \left[\frac{e^{-y^2}}{\sqrt{\pi}[1 + \text{erf}(y)]} + y \right]^{-1} \quad (36)$$

is the scaling function of the scaling parameter,

$$y = \frac{2\alpha - 1}{\sqrt{t}}. \quad (37)$$

Equation (36) represents the analytical expression for the scaling function $f(y)$ shown in Fig. 3. This function defines the magnetization curve and the zero-field susceptibility,

$$\chi(t, \alpha) = \frac{1}{3t^{3/2}} f(y). \quad (38)$$

The behavior of the scaling function $f(y)$ defines two regions with different types of thermodynamics. The first region corresponds to the limit $y \rightarrow -\infty$, where the scaling function $f(y)$ tends to the asymptotic $f(y) = -2y$ and the gravitational

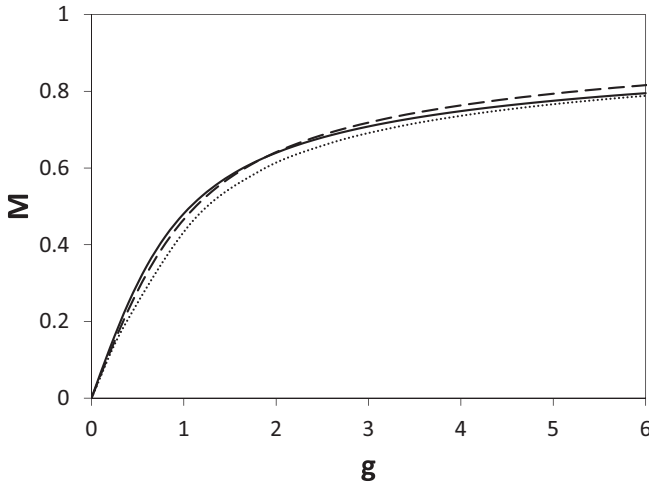


FIG. 4. Magnetization curve obtained by numerical solution of the integral equation (25) and plotted as a function of the scaled magnetic field g (35) for $\alpha = 0.2$ (dotted line) and $\alpha = 0.5$ (dashed line) and $t = 0.1$ in comparison with the scaling function $\phi(g)$ (solid line) representing the exact result in the $t \rightarrow 0$ limit.

field g is

$$g = \frac{1 - 2\alpha}{t^2} h. \quad (39)$$

This region is limited by the condition $(1 - 2\alpha) \gg \sqrt{t}$ and extends up to the pure ferromagnetic case $\alpha = 0$. Therefore, we name this region the “ferromagnetic” regime. The thermodynamics in the ferromagnetic regime is similar to that for the ferromagnetic chain. In particular, the zero-field susceptibility behaves as $\chi \sim t^{-2}$.

The second region is located near the critical point $\alpha = \frac{1}{2}$ and is restricted by the condition $|1 - 2\alpha| \ll \sqrt{t}$ ($|y| \ll 1$). In this “critical point” region, one can take the limit $f(0) = \sqrt{\pi}$ and the gravitational field becomes

$$g = \frac{\sqrt{\pi}}{2t^{3/2}} h. \quad (40)$$

The thermodynamics in this region is governed by the critical point. In particular, the zero-field susceptibility behaves as $\chi \sim t^{-3/2}$. The crossover between these two regimes takes place at the value $y \simeq -1$, or $t \simeq t_0 = (1 - 2\alpha)^2$.

If we study the low- t thermodynamics of the classical Δ -chain for some fixed value of α (not far from the transition point), the above two regimes will manifest as follows. The ferromagnetic regime taking place at very low temperatures $t \ll t_0$ will gradually be replaced by the critical point regime for $t \gg t_0$ (but still $t \ll 1$).

The scaling function $\phi(g)$ describes the magnetization in $t \rightarrow 0$ limits. However, the comparison of the exact numerical solution of Eq. (25) for $\alpha = 0.2$ and $\alpha = 0.5$ with the scaling function given by Eq. (34) shows a good agreement of both results even for $t = 0.1$, as shown in Fig. 4.

The comparison of the classical with the experimental magnetization curves for $\text{Fe}_{10}\text{Gd}_{10}$ is shown in Fig. 5. We find a reasonable agreement. The slight differences between the theoretical and the experimental curves can be attributed to

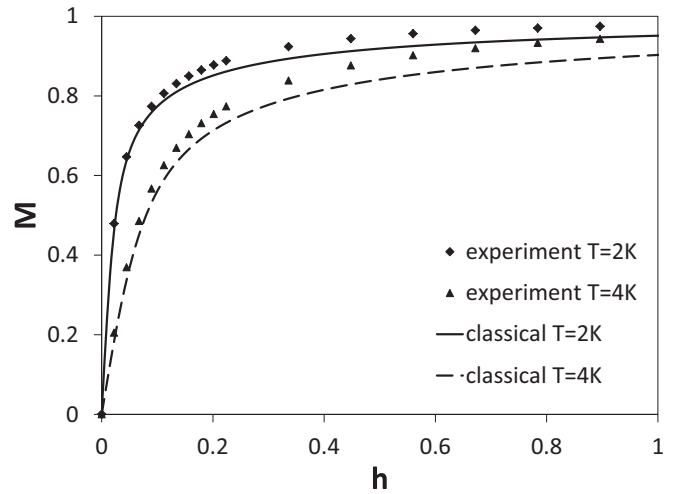


FIG. 5. Magnetization curve obtained by numerical solution of the integral equation (25) for $\alpha = 0.45$ in comparison with the experimental data for $\text{Fe}_{10}\text{Gd}_{10}$ for $T = 2$ and $T = 4$ K. The real magnetic field B is converted to the normalized h by the equation $h = g\mu_B B / Jsk_B$ and the normalized temperature relates to the real temperature by $t = T / Js(s + 1)$, with $s = 3$ and $J = 2$ K [18].

quantum effects and to different apical and basal spins present in $\text{Fe}_{10}\text{Gd}_{10}$.

2. Ferrimagnetic region $\alpha > \frac{1}{2}$

In the ferrimagnetic region, the neighboring basal spin vectors form an angle $2\theta_0$ in the ground state, as shown in Fig. 2. In the vicinity of the transition point $(\alpha - \frac{1}{2}) \ll 1$, the angle $\theta_0 \ll 1$ [Eq. (10)], so that the ground state is close to the ferromagnetic one. In this case, the approach developed in the previous section remains valid. This means that on the ferrimagnetic side of the transition point (and close to it), the magnetization curve is given by the same scaling function $\phi(g)$, with g defined by Eq. (35). The behavior of the scaling function $f(y)$ for $y > 0$ exhibits two low- t regimes. The critical point regime discussed in the previous section extends to the ferrimagnetic region and is restricted by the condition $(2\alpha - 1) \ll \sqrt{t}$ ($y \ll 1$). In the limit $y \gg 1$, the scaling function behaves as $f(y) \sim 1/y$, which means that for very low temperature $t \ll (2\alpha - 1)^2$, the system is in the ferrimagnetic regime with different thermodynamic exponents. In particular, the temperature dependence of the susceptibility in this case is $\chi \sim t^{-1}$.

We stress that the above scaling approach is valid in the vicinity of the transition point only, where $\theta_0 \ll 1$. Far from the transition point, the angle θ_0 is no longer small, and in order to describe the low-temperature thermodynamics, one needs to expand the local Hamiltonian near the ferrimagnetic ground-state configuration described by Eq. (10). The magnetization curve in the ferrimagnetic ground state (11) and for several small values of t for $\alpha = 1$ is shown in Fig. 6. As can be seen, the magnetization curves approach the ground-state curve with decreasing t . According to Fig. 6, the magnetization curves have three different scales in the magnetic field which should be studied separately: $h \ll t$, $t < h < h_{\text{sat}}$, and $h \geq h_{\text{sat}}$.

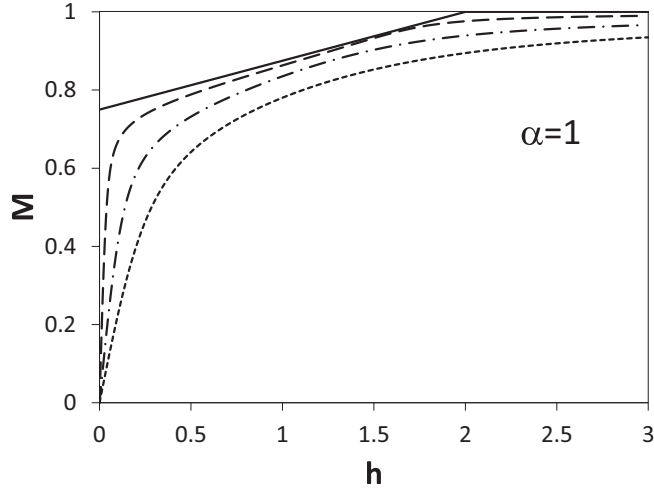


FIG. 6. Magnetization curves for $\alpha = 1$ and several temperatures $t = 0.03$ (dashed line), $t = 0.1$ (dot-dashed line), and $t = 0.2$ (dotted line), obtained by numerical solution of the integral equation (25). The ground-state magnetization curve (11) is shown by a solid line.

For very low magnetic field $h \ll t$, the ground-state spin configurations can be described in terms of finite-step random walk on the unit sphere in a weak gravitational field [20]. The magnetization in this case increases linearly with the magnetic field and the zero-field susceptibility was calculated in Ref. [20]:

$$M = \chi h, \quad (41)$$

$$\chi = \frac{1}{6t} \frac{2\alpha + 1}{2\alpha - 1}. \quad (42)$$

Then, for higher magnetic field $t < h < h_{\text{sat}}$, the magnetization approaches its ground-state value (11), and the integral equation (31) can be solved using the saddle-point approximation. For this aim, we introduce small deviations $\delta_1, \delta_3, \varepsilon$ from the ferrimagnetic ground state (10):

$$\cos \theta_1 = \cos \theta_0 + \delta_1, \quad \cos \theta_3 = \cos \theta_0 + \delta_3, \quad \varphi = \pi + \varepsilon. \quad (43)$$

The leading terms of the expansion of the local Hamiltonian in $\delta_1, \delta_3, \varepsilon$ are

$$\mathcal{H}_{13} = E_{\text{gs1}} + A_1(\delta_1^2 + \delta_3^2) + 2B_1\delta_1\delta_3 + C_1\varepsilon^2, \quad (44)$$

where

$$E_{\text{gs1}} = -\frac{(2+h)^2}{8\alpha} - h - \alpha, \quad (45)$$

$$A_1 = \frac{8\alpha^3(2\alpha h + h + 2) - \alpha(h + 2)^2}{[16\alpha^2 - (h + 2)^2](2\alpha h + h + 2)}, \quad (46)$$

$$B_1 = A_1 - \frac{\alpha h(2\alpha + 1)(h + 2)^2}{[16\alpha^2 - (h + 2)^2](2\alpha h + h + 2)}, \quad (47)$$

$$C_1 = \frac{h(2\alpha + 1)[16\alpha^2 - (h + 2)^2]}{32\alpha(2\alpha h + h + 2)}. \quad (48)$$

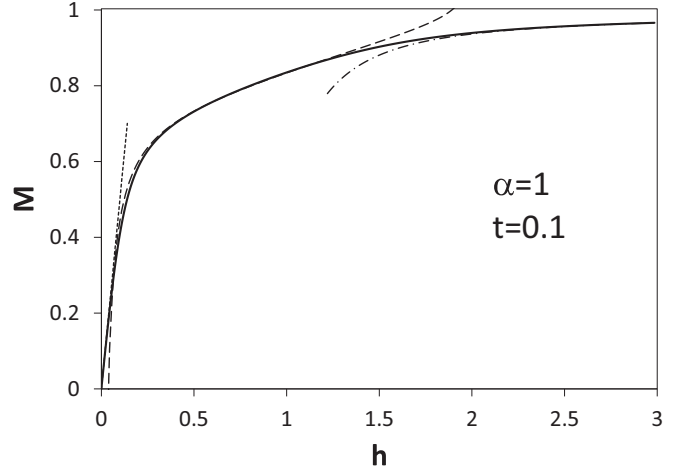


FIG. 7. Magnetization curves for $\alpha = 1$ and $t = 0.1$ obtained by numerical solution of the integral equation (25) (solid line) and approximate equations (41), (49), and (55) in the corresponding regions (dashed lines).

The solution of the integral equation (31) in this case is

$$\lambda = \exp\left(-\frac{E_{\text{gs1}}}{t}\right) \frac{\pi t^2}{h_{\text{gs}} \sqrt{A_1 C_1 + C_1 \sqrt{A_1^2 - B_1^2}}}. \quad (49)$$

The magnetization is given by the relation

$$M = t \frac{\partial \ln \lambda}{\partial h}. \quad (50)$$

Finally, when the magnetic field is higher than the saturation one, $h > h_{\text{sat}}$, the ground state becomes ferromagnetic and the magnetization only slightly differs from its fully saturated value. This means that the angles θ_1 and θ_3 are small and the expansion of the local Hamiltonian becomes

$$\mathcal{H}_{13} = E_{\text{gs2}} + A_2(\theta_1^2 + \theta_3^2) + 2B_2\theta_1\theta_3 \cos \varphi, \quad (51)$$

$$E_{\text{gs2}} = -2 + \alpha - 2h, \quad (52)$$

$$B_2 = \frac{1}{2} \left(\alpha - \frac{1}{2+h} \right), \quad (53)$$

$$A_2 = B_2 + \frac{h - h_{\text{sat}}}{4}. \quad (54)$$

In this case, after some algebra, the solution of the integral equation (31) yields the partition function

$$\lambda = \frac{1}{8A_2} \frac{t^2}{2+h} \exp\left(-\frac{E_{\text{gs2}}}{t}\right) \left(1 + \frac{B_2^2}{4A_2^2}\right). \quad (55)$$

As shown in Fig. 7 for $\alpha = 1$, Eqs. (41), (49), (50), and (55) perfectly describe the magnetization curve in the corresponding regions of the magnetic field.

III. QUANTUM EFFECTS

In the preceding section, we presented results for the classical delta-chain in the magnetic field. Since the classical model corresponds to the limit $s \rightarrow \infty$, a natural question arises about the relation of the classical results to those of

the quantum spin- s model (1). In this respect, it is important to mention Ref. [27], where it was conjectured that the magnetization curves of the quantum and classical ferromagnetic chain coincide in the low-temperature limit and are described by a universal function $\phi(g_F)$, given by Eq. (33), of the scaling variable g_F ,

$$g_F = \frac{s^3 H}{T^2}. \quad (56)$$

In this section, we will use the nonrenormalized temperature $T = ts^2$ and the magnetic field $H = sh$. As the ferromagnetic chain corresponds to the particular case $\alpha = 0$ of our model, the problem of ‘‘universality’’ of the classical results for $\alpha > 0$ will be the focus of our attention. Additional motivation to study the quantum effects to the classical results is that $\text{Fe}_{10}\text{Gd}_{10}$ is described by the quantum model with relatively high, but nevertheless finite, spin values. For the analysis of the magnetic properties of the quantum spin model, we investigate finite chains imposing periodic boundary conditions using the numerical exact diagonalization (ED) [21] and the finite-temperature Lanczos (FTL) technique [22,23].

A. Transition point

We start our analysis from the transition point $\alpha = \frac{1}{2}$. The spin- $\frac{1}{2}$ case of quantum model (1) at the transition point was studied in detail in Ref. [13]. It was shown that this model has many very specific properties: a flat one-magnon spectrum, localized one-magnon states and multimagnon complexes, a macroscopic degeneracy of the ground state and a residual entropy, exponentially low-lying excitations, and a multiscale structure of the energy spectrum [14]. It turns out that all of these specific properties of the spin- $\frac{1}{2}$ model carry over to the models with higher values of spin with some inessential modifications, which we will briefly describe below.

The ground state of the quantum delta-chain with any value of s at the critical point $\alpha = \frac{1}{2}$ consists of exact multimagnon bound states, exactly like the $s = \frac{1}{2}$ model and the number of the ground states, $B_{N/2}^k$, for fixed value $S^z = S_{\max} - k$, $S_{\max} = sN$, is [13]

$$B_{N/2}^k = C_{N/2}^k, \quad 0 \leq k \leq \frac{N}{4}, \quad 2S_{\max} - \frac{N}{4} < k \leq 2S_{\max},$$

$$B_{N/2}^k = C_{N/2}^{N/4}, \quad \frac{N}{4} + 1 \leq k \leq 2S_{\max} - \frac{N}{4},$$

where $C_m^n = \frac{m!}{n!(m-n)!}$ is the binomial coefficient.

The contribution to the partition function from only these degenerate ground states is

$$Z_{\text{GS}} = \sum_k B_{N/2}^k \exp \left[\frac{(S_{\max} - k)H}{T} \right]. \quad (57)$$

Using a saddle-point approximation to the estimate of Eq. (57), we obtain the corresponding normalized magnetization in the form

$$M_{\text{GS}} = 1 - \frac{1}{2s[1 + \exp(H/T)]}. \quad (58)$$

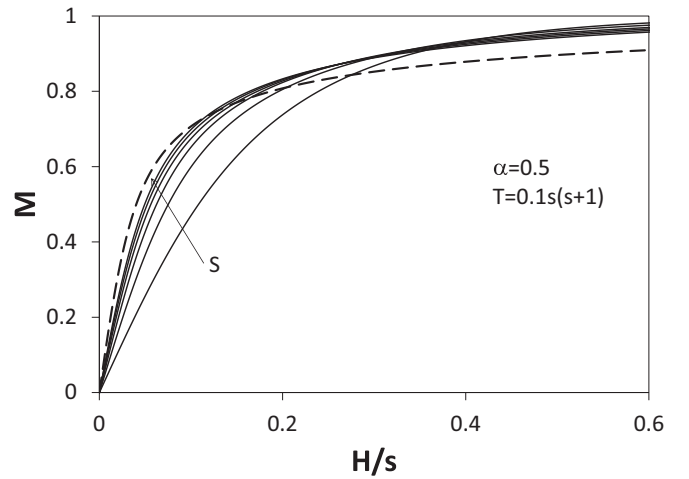


FIG. 8. Magnetization curves $M(H/s)$ for the quantum models with $s = \frac{1}{2}$ ($N = 36$), $s = 1$, $\frac{3}{2}$ ($N = 16$), and $s = 2$, $\frac{5}{2}$, 3 ($N = 12$) (solid lines) at the transition point $\alpha = \frac{1}{2}$ for $T/s(s+1) = 0.1$. The magnetization curve of the classical model for $\alpha = \frac{1}{2}$ and $t = 0.1$ is shown by the dashed line.

As follows from Eq. (58), the magnetization at the critical point for $H \rightarrow 0$ is

$$M_{\text{GS}} = 1 - \frac{1}{4s}, \quad (59)$$

and it changes from $M_{\text{GS}} = \frac{1}{2}$ for $s = \frac{1}{2}$ to $M_{\text{GS}} = 1$ for the classical limit $s \rightarrow \infty$.

According to Eq. (59), the magnetization M_{GS} is finite for $H \rightarrow 0$, which would clearly contradict the statement that long-range order cannot exist in one-dimensional systems at $T > 0$. For the correct description of $M(H, T)$, it is thus necessary to take into account the full spectrum of the model. Unfortunately, such analytical calculation is impossible, and we therefore carried out ED and FTL calculations of $M(H, T)$ for different values of s and N . The corresponding results together with that for the classical model are shown in Fig. 8. As can be seen in Fig. 8, the behaviors of the classical and quantum model are very different. This implies that there is no universality at the critical point. At the same time, there is one interesting point related to the behavior of the magnetization at low magnetic field. It was shown in Ref. [13] that the magnetization of the $s = \frac{1}{2}$ delta-chain is $M \sim H/T^\gamma$ with an exponent $\gamma = 1.09$. On the other hand, in the classical model ($s \rightarrow \infty$), $\gamma = \frac{3}{2}$ according to Eq. (38). Therefore, it can be expected that the exponent γ is a function of s . To clarify this point, we have calculated the zero-field susceptibility χ for different s and N . The dependencies $\chi(T)$ are shown in Fig. 9 as a log-log plot of $3\chi T/s(s+1)$ vs $T/s(s+1)$. The solid lines denote, from bottom to top, $s = \frac{1}{2}$ ($N = 36$), $s = 1$ ($N = 16$), and $s = \frac{3}{2}$, 2 , $\frac{5}{2}$, 3 with $N = 12$. The classical curve is shown by a dashed line. As can be seen in Fig. 9, all curves tends to 1 in the high-temperature limit, which is in accord with the high- T behavior of the susceptibility $\chi = s(s+1)/3T$. Then, for lower temperature, all curves diverge from each other and, in a definite intermediate-temperature region, the curves have linear behavior with different slope,

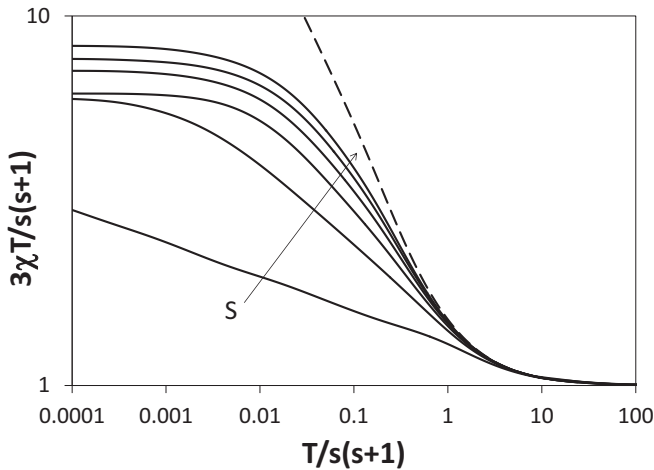


FIG. 9. Log-log plot for the dependence of $3\chi T/s(s+1)$ on the normalized temperature $T/s(s+1)$ for the classical (dashed line) and quantum spin- s (solid lines) delta-chain calculated at the critical point $\alpha = 0.5$.

which implies a power-law dependence,

$$\chi = r(s)/T^{\gamma(s)}. \quad (60)$$

This means that the low-field behavior of the magnetization is $M \sim H/T^{\gamma(s)}$. The dependence of the critical exponent on spin value $\gamma(s)$ is shown in Fig. 10 and it can be seen that $\gamma \rightarrow \frac{3}{2}$ in the classical limit $s \gg 1$. When further decreasing $T/s(s+1)$ for all solid curves, the sloping part in Fig. 9 is followed by a flat part related to finite-size effects. At $T \rightarrow 0$, the solid curves tend to the values determined by the contributions of the degenerate ground states. These contributions for finite delta-chains can be found by the calculations of the zero-field susceptibility per spin using Eq. (57), which results in

$$\chi = \frac{c_N(s)N}{T}, \quad (61)$$

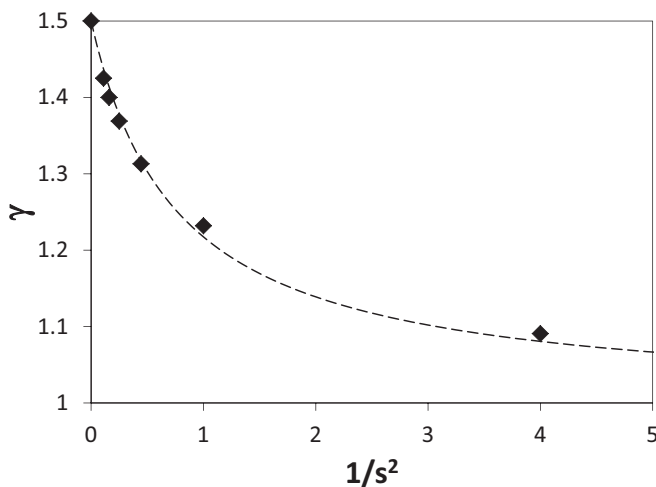


FIG. 10. Dependence of the critical exponent γ on the spin value s . The dashed line represents the approximate expression $\gamma = \frac{3s^2+2.6}{2s^2+2.6}$.

where $c_N(s) = \frac{1}{2}(s - \frac{1}{4})^2$ for $N \gg 1$. We suppose that both Eqs. (60) and (61) for $\chi(T)$ are described by a single finite-size scaling function, which has the form [13]

$$\chi(T) = T^{-\gamma} F(c_N(s)NT^{\gamma-1}). \quad (62)$$

For small x , the function $F(x)$ gives (61) and, in the thermodynamic limit $N \rightarrow \infty$, the scaling function tends to the value $r(s)$ in accord with Eq. (60). The crossover between these two types of susceptibility behavior occurs at $x \simeq 1$, which defines the crossover temperature $T^* \sim N^{-1/(\gamma-1)}$. At $T < T^*$, finite-size effects are essential and χ is given by Eq. (61). The crossover temperature T^* increases with s and the region of finite-size behavior of χ increases.

B. Ferromagnetic phase

As was noted in the beginning of this section, in the special case $\alpha = 0$, the magnetization curves of both quantum and classical delta-chain models coincide in the low-temperature limit. According to the scaling hypothesis [27], the normalized magnetization M for the infinite chain is expressed at $T \rightarrow 0$ and $\frac{h}{T} \rightarrow 0$ [but with fixed g_F (56)] as $M(T, h) = \phi(g_F)$ and the function $\phi(g_F)$ is obtained by calculating the eigenspectrum of the quantum rotator Hamiltonian (32) in the gravitational field g_F . As noted in Ref. [27], the hypothesis of universality originates in the universal behavior of the spin-wave excitations above the ferromagnetic ground state in both quantum and classical models. Similarly to the case $\alpha = 0$, one can expect that such universality remains in the ferromagnetic part of the ground-state phase diagram ($\alpha < \frac{1}{2}$), with g_F in Eq. (56) being replaced by

$$g_F = \frac{(1-2\alpha)s^3H}{T^2}, \quad (63)$$

in accordance with Eq. (39) for the classical model.

The universality for $\alpha < \frac{1}{2}$ is partly confirmed by the fact that the leading terms of the zero-field susceptibility at $T \rightarrow 0$ for the classical model and that obtained using modified spin-wave theory [29] for the quantum model coincide [20]. Unfortunately, modified spin-wave theory is restricted to zero magnetic field, and it cannot confirm the universality of the magnetization curve.

However, the extension of the hypothesis of universality for the case $\alpha \neq 0$, and especially for α close to the transition point $\alpha = \frac{1}{2}$, needs some comments. As shown in the preceding section, the scaling parameter g in the classical model has two different forms, given by Eqs. (39) and (40), for $T \ll T_0$ and $T \gg T_0$, respectively, where $T_0 = (1-2\alpha)^2s^2$ is the temperature of the crossover. For $T \ll T_0$, this parameter takes the form (63), while for $T \gg T_0$, it corresponds to that for the transition point regime, where the behavior of the classical and quantum models is very different. Therefore, one can expect that there is identical universality of the classical and quantum models in the low-temperature region $T \ll T_0$ only.

The quantum models also have different low-temperature regimes when α is close to the transition point. As an example, we show in Fig. 11 the dependence of the susceptibility for the $s = \frac{1}{2}$ delta-chain and $\alpha = 0.45$ with $N = 32$ and $N = 36$ obtained by FTL calculations, where for convenience we

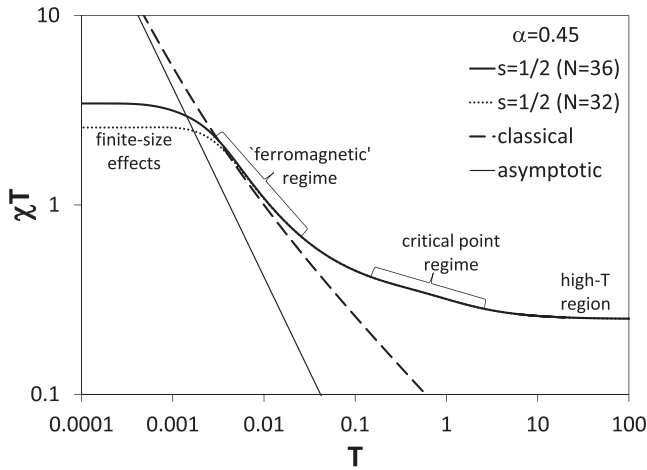


FIG. 11. Susceptibility times temperature, χT , in dependence on T for $\alpha = 0.45$ obtained numerically by FTL for $s = 1/2$ and $N = 32$ (dotted line), $N = 36$ (thick solid line). The classical curve is shown by the dashed line. The thin solid line describes low- T asymptotic $\chi = (1 - 2\alpha)/24T^2$.

represent this dependence as a log-log plot of $T\chi(T)$. At first, we note that the curves with $N = 32$ and $N = 36$ perfectly coincide for $T > 0.003$, which means that they correctly describe the thermodynamic limit in this region. In the high-temperature limit, the curves tend to a constant, which implies the correct asymptotic $\chi(T) = 1/(4T)$. In the temperature range $0.1 \lesssim T \lesssim 3$, the slope of the curve is very close to that obtained for $s = \frac{1}{2}$ at the transition point [13]: $\chi(T) \sim T^{-\gamma}$ with $\gamma = 1.09$. Therefore, we refer this region to the critical point regime.

For temperatures lower than the critical point region, the slope of the curves increases and, after some crossover region, the quantum curves approach the classical curve, as shown in Fig. 11 by a dashed line. We name the region where the quantum curves are close to the classical one, $0.003 \lesssim T \lesssim 0.02$, the “ferromagnetic” one. Though the slope of the curves in this region corresponds to $\gamma \sim 1.7$ instead of a ferromagnetic $\gamma = 2$, we see that all curves converge to the ferromagnetic low- T asymptotic $\chi = (1 - 2\alpha)/24T^2$, shown by the thin solid line in Fig. 11. For $T < 0.003$, the quantum curves for $N = 32$ and $N = 36$ diverge from each other and both from the classical curve, establishing the “finite-size effect” region with nonthermodynamic behavior. Looking at Fig. 11, it is natural to assume that the quantum curve corresponding to very long chains would go further into the lower- T region close to the classical curve and both asymptotically approach the thin solid line, i.e., the ferromagnetic law $\chi = (1 - 2\alpha)/24T^2$. This means that for the infinite delta-chain, the ferromagnetic region exists up to $T = 0$. Unfortunately, for $\alpha \neq 0$, the quantum models can be studied only by numerical calculations of finite delta-chains, which, due to finite-size effects, complicates the study of the low-temperature region.

The magnetization curves in the ferromagnetic temperature region for the $s = \frac{1}{2}$ model with $N = 36$ and for $\alpha = 0.45$ obtained by numerical FTL calculations are shown in Fig. 12 as a function of the ferromagnetically scaled field g_F (63). In Fig. 12, we also show the scaling function $\phi(g)$. As can be

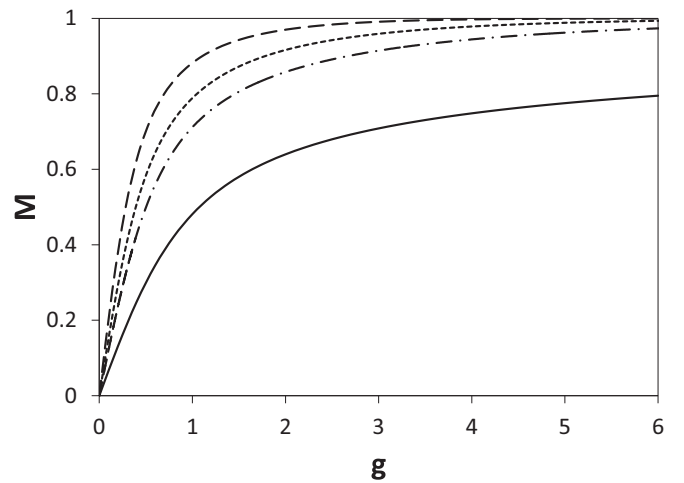


FIG. 12. Magnetization curve for $\alpha = 0.45$ obtained numerically by FTL for $s = 1/2$, $N = 36$ and three different temperatures located in the ferromagnetic region of Fig. 11: $T = 0.004$ (dash-dotted line), $T = 0.0075$ (short-dashed line), and $T = 0.015$ (long-dashed line). The data are plotted as a function of the scaled magnetic field g_F (63). The exact universal magnetization curve $\phi(g_F)$ is shown by the solid line.

seen, the quantum magnetization curves tend to the scaling function as the temperature decreases. However, the difference between these curves and $\phi(g)$ is rather appreciable. The point is that the function $\phi(g)$ represents the leading term in the low-temperature expansion of the magnetization. The temperatures corresponding to the magnetization of the $s = \frac{1}{2}$ model in Fig. 12 are about T_0 . At such a temperature, the next terms in the low-temperature expansion of the magnetization are of the same order as the leading term. This appreciable difference of the initial slope of the quantum magnetization curve and $\phi(g)$ can also be seen in Fig. 11: in the ferromagnetic region, the values $\chi(T)$ for the quantum curve are approximately two times larger than that for the asymptotic line corresponding to the initial slope of $\phi(g)$. The comparison of the classical and asymptotic lines in Fig. 11 shows that the difference would become $\sim 10\%$ for $T \lesssim 0.0005$, but, in order to avoid the finite-size effects at such low temperatures, one needs to calculate very long chains.

In the finite-size region, the correlation length $\xi = (1 - 2\alpha)s^2/T$ is much larger than the system size accessible in exact diagonalization (ED) ($N \sim 24$) or FTL ($N \sim 36$) calculations (especially for α close to $\frac{1}{2}$). In this region, the finite-size effects are essential and the scaling function for the magnetization depends on two parameters $\phi(g_F, q)$ [27], with

$$q = \frac{(1 - 2\alpha)s^2}{TN}. \quad (64)$$

At $T \rightarrow 0$ and $q \gg 1$, the function $\phi(g, q)$ is given by the Langevin equation

$$M = \phi(g_F, q) = \coth(x) - \frac{1}{x}, \quad (65)$$

with

$$x = \frac{g_F}{q} = \frac{NsH}{T}. \quad (66)$$

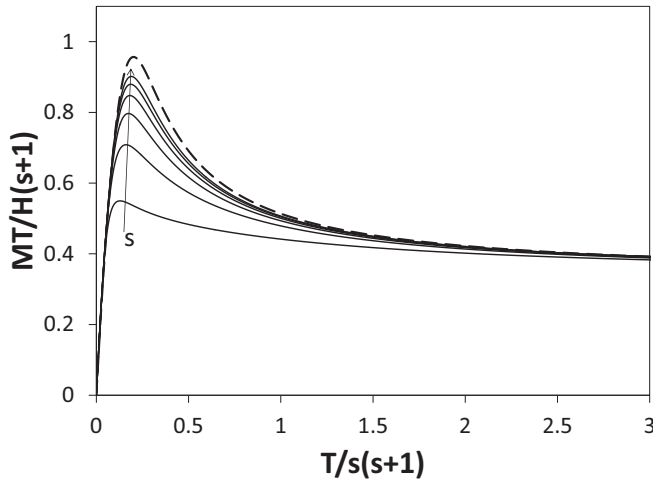


FIG. 13. Comparison of quantum (solid lines) and classical (dashed line) dependencies $MT/H(s+1)$ vs $T/s(s+1)$ calculated for $\alpha = 0.45$ and $h = 0.1$. The curves with spin $s = \frac{1}{2}, 1, \frac{3}{2}, 2, \frac{5}{2}, 3$ are arranged in order from bottom to top.

The magnetization calculated for the quantum delta-chain at $\alpha = 0.45$ with $s = \frac{1}{2}$ and $N = 36$ agrees well with Eq. (65).

The numerical calculations of the magnetization of the quantum $s = \frac{1}{2}$ model for temperatures $T \gg T_0$ show significant difference from the classical scaling function $\phi(g)$ (we note that the above statement is restricted by low temperature, $T < 1$, where the scaling arguments can be applied). Therefore, we conclude that the magnetization for $0 \leq \alpha < \frac{1}{2}$ is a universal function for both the quantum and classical delta-chain only in the ferromagnetic regime ($T \ll T_0$).

As discussed in Secs. I and II C 1, the classical approximation for the F-AF delta-chain is justified for $\text{Fe}_{10}\text{Gd}_{10}$ because the spin quantum numbers for Fe and Gd ions are rather large. The characteristic feature related to the susceptibility of $\text{Fe}_{10}\text{Gd}_{10}$ is a maximum in the temperature dependence of the quantity MT/H in a fixed magnetic field. The calculation of this quantity for the classical model shows good agreement with the experimental data. In particular, the maximum $(MT/H)_{\text{max}} \sim 720 \text{ cm}^3 \text{ K/mol}$ is reached at $T_{\text{max}} \sim 4 \text{ K}$ in comparison with the experimental data $(MT/H)_{\text{max}} \sim 745 \text{ cm}^3 \text{ K/mol}$ reached at $T_{\text{max}} \sim 3 \text{ K}$. The temperature dependence of MT/H for quantum models with different values of spin s is shown in Fig. 13 together with that for the classical model. As can be seen in Fig. 13, the dependencies MT/H approach the classical curve as s increases.

C. Ferrimagnetic phase

The ground state of the classical model is ferrimagnetic at $\alpha > \frac{1}{2}$. As we noted before, in Ref. [11], it was stated that a ferrimagnetic ground-state phase is also realized for the $s = \frac{1}{2}$ quantum delta-chain. At the same time, the behavior of the magnetization curve of the classical and quantum models is very different, as shown in Fig. 14 for $\alpha = 1$. It is possible to state with certainty that there is no universality in this phase. At present, not much is known about the ground-state phase of the quantum models with $s > \frac{1}{2}$ and this problem needs further study. One interesting point is the dependence

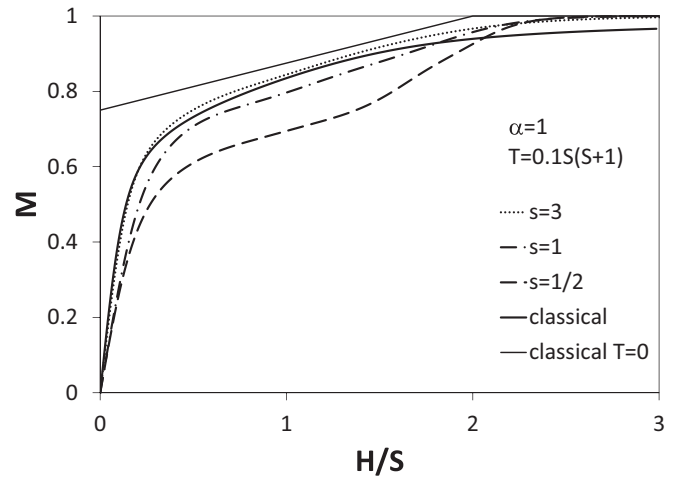


FIG. 14. Comparison of the magnetization curves $M(H/s)$ for the classical (thick solid line) and quantum models with $s = 1/2, N = 36$ (dashed line), $s = 1, N = 16$ (dash-dotted line), and $s = 3, N = 12$ (dotted line) in the ferrimagnetic region $\alpha = 1$ for $T/s(s+1) = 0.1$. The ground-state magnetization curve of the classical model (11) is shown by the thin solid line.

of the magnetization behavior on s . As shown in Fig. 14, the magnetization curves rapidly approach the classical one when s increases. It can be expected that the magnetization of the quantum model in the limit $s \gg 1$ will coincide with the classical curve.

Another interesting problem is the limit $\alpha \gg 1$, where the antiferromagnetic basal chain is weakly connected to the apical spins. In this limit, the behavior of the system can be qualitatively different for integer and half-integer basal spins due to the Haldane gap in the spectrum of the basal subsystem. In this respect, one should be cautious because the replacement of basal spin $s = \frac{7}{2}$ to $s = 3$ would lead to qualitatively wrong results. However, this problem is beyond the scope of this paper because the experimental value of $\alpha = 0.45$ is very far from the limit $\alpha \gg 1$.

IV. SUMMARY

In this paper, we have studied the delta-chain with competing ferro- and antiferromagnetic interactions J_1 and J_2 in the external magnetic field. At $\alpha = J_2/|J_1| = 1/2$, this model belongs to the class of flat-band models exhibiting a massively degenerated ground state leading to a residual entropy. Since a magnetic field partially lifts the degeneracy, the influence of the field on the low-temperature physics is tremendous. Interestingly, there is a finite-size realization of the model, namely, the magnetic molecule $\text{Fe}_{10}\text{Gd}_{10}$, which has J_1 and J_2 close to the flat-band point. In the present study, for the classical model, exact results for the thermodynamics are obtained. It is shown that the calculation of the magnetization for $\alpha \leq \frac{1}{2}$ in the limit $T \rightarrow 0$ and $\frac{H}{T} \rightarrow 0$ reduces to the solution of the Schrödinger equation for the quantum rotator in the gravitational field g , which depends on the temperature. The low-temperature region of the classical model consists of two regions $T \ll T_0$ and $T \gg T_0$ [$T_0 \sim (1 - 2\alpha)^2 s^2$] with different type of $g(T)$ dependence. The magnetization for

$T \ll T_0$ is a universal function of the scaling parameter g , which is valid for both the classical and quantum models. In particular, the susceptibility behaves as $\chi \sim T^{-2}$. For $T \gg T_0$, the behavior of the magnetization and the susceptibility is the same as in the critical point $\alpha = \frac{1}{2}$ and it is different for the classical and the quantum models. In this case, the susceptibility of the classical model behaves as $\chi \sim T^{-3/2}$, while $\chi \sim T^{-\gamma}$ with $\gamma = 1.09$ for the quantum $s = \frac{1}{2}$ model. Generally, the value of the exponent γ depends on s and it tends to the classical value $\gamma = \frac{3}{2}$ when s increases.

We compare the obtained results with the experimental data for $\text{Fe}_{10}\text{Gd}_{10}$, which is a finite-size realization of the considered model with $\alpha \simeq 0.45$. We show that the magnetization $M(H)$ of both the classical and quantum models with $s = 3$ agrees well with the experimental magnetization curves measured at $T = 2$ and $T = 4$ K. We also discuss the maximum in the temperature dependence of the quantity MT/H at fixed magnetic field and show that it agrees very well with the experimentally observed one.

APPENDIX

In the ferromagnetic region $\alpha < \frac{1}{2}$ including the vicinity of the critical point $\alpha = \frac{1}{2}$ at low t , nearest-neighbor spins \vec{n}_1 and \vec{n}_3 are almost parallel. In the pure ferromagnetic case $\alpha = 0$, the angle between the neighboring spin vectors is of the order of $t^{1/2}$ and the magnetic field scales as $h \sim t^2$ [27]. As was pointed out in Ref. [20], near the critical point the critical properties change so that the angle between the neighboring spin vectors is of the order of $t^{1/4}$ and, as will be shown below, the magnetic field scales as $h \sim t^{3/2}$ in the low- t limit. Using these facts, we expand the effective magnetic field acting on the apical spin as

$$h_a \approx 2 - \frac{1}{2}(1 - \vec{n}_1 \cdot \vec{n}_3) - \frac{1}{16}(1 - \vec{n}_1 \cdot \vec{n}_3)^2 + \frac{1}{2}\vec{h} \cdot (\vec{n}_1 + \vec{n}_3). \quad (\text{A1})$$

This results in the following effective local Hamiltonian (29):

$$\mathcal{H}_{13} = \left(\frac{1}{2} - \alpha\right)(1 - \vec{n}_1 \cdot \vec{n}_3) + \frac{1}{16}(1 - \vec{n}_1 \cdot \vec{n}_3)^2 - \vec{h} \cdot (\vec{n}_1 + \vec{n}_3). \quad (\text{A2})$$

Though the second term in Eq. (A2) is of the second order in the small parameter $(1 - \vec{n}_1 \cdot \vec{n}_3)$, it becomes relevant in the vicinity of the critical point when the factor $(\frac{1}{2} - \alpha)$ at the first-order term is small.

Next, we can simplify Eq. (31) by substituting $h_{gs} = 2$ from Eq. (27), and expanding the exponent with the magnetic field term ($\beta h \ll 1$),

$$\exp[\beta h(n_1^z + n_3^z)] \approx 1 + \beta h(n_1^z + n_3^z) \approx 1 + 2\beta h n_3^z, \quad (\text{A3})$$

which transforms Eq. (31) into the form

$$(1 + 2\beta h n_3^z) \int e^{-\beta \mathcal{H}(\vec{m})} \psi(\vec{n}_3 + \vec{m}) d\vec{m} = 4\beta \lambda \psi(\vec{n}_3), \quad (\text{A4})$$

where

$$\mathcal{H}(\vec{m}) = \frac{1 - 2\alpha}{4} \vec{m}^2 + \frac{1}{64} (\vec{m}^2)^2, \quad (\text{A5})$$

and

$$\vec{m} = \vec{n}_1 - \vec{n}_3 \quad (\text{A6})$$

is a small vector of length $|\vec{m}| \sim t^{1/4}$, which can be considered as a 2D vector (m_1, m_2) in the plane perpendicular to the spin vector \vec{n}_3 .

Now we expand the function ψ in Eq. (A4) to the second order in \vec{m} :

$$\psi(\vec{n} + \vec{m}) = \psi(\vec{n}) + m_i \frac{\partial \psi(\vec{n})}{\partial n_i} + \frac{1}{2} m_i m_j \frac{\partial^2 \psi(\vec{n})}{\partial n_i \partial n_j}, \quad (\text{A7})$$

where derivatives are taken along two orthogonal directions in the plane perpendicular to the spin vector \vec{n} .

The Hamiltonian (A5) is a function of \vec{m}^2 . Therefore, linear terms in m_i and terms $\sim m_1 m_2$ in Eq. (A7) vanish after integration over \vec{m} in the integral equation (A4). As a result, the integral equation (A4) becomes

$$(1 + 2\beta h n_3^z) \psi(\vec{n}) \int e^{-\beta \mathcal{H}(\vec{m})} d\vec{m} + \frac{1}{4} \frac{\partial^2 \psi}{\partial n_i^2} \int e^{-\beta \mathcal{H}(\vec{m})} \vec{m}^2 d\vec{m} = 4\beta \lambda \psi(\vec{n}), \quad (\text{A8})$$

where we omit the next-order terms $\sim \beta h \vec{m}^2$. Now we notice that

$$\frac{\partial^2}{\partial n_1^2} + \frac{\partial^2}{\partial n_2^2} = -\hat{L}^2 \quad (\text{A9})$$

is simply the angular momentum operator. Therefore, we come to the Schrödinger equation for the quantum rotator in the gravitational field,

$$\left(\frac{1}{2}\hat{L}^2 - g n_3^z\right) \psi(\vec{n}) = \mu \psi(\vec{n}), \quad (\text{A10})$$

where the gravitational field

$$g = \frac{A}{B} \beta h \quad (\text{A11})$$

depends on the Hamiltonian $\mathcal{H}(\vec{m})$ via the integrals A and B :

$$A = \int e^{-\beta \mathcal{H}(\vec{m})} d\vec{m},$$

$$B = \frac{1}{4} \int e^{-\beta \mathcal{H}(\vec{m})} \vec{m}^2 d\vec{m}, \quad (\text{A12})$$

and the partition function λ is given by the lowest eigenvalue μ_0 by the equation

$$\lambda = \frac{A - 2B\mu_0}{4\beta}. \quad (\text{A13})$$

Calculating A and B in Eq. (A12) for $\mathcal{H}(\vec{m})$ given by Eq. (A5), we have

$$g = \frac{h}{2t^{3/2}} f(y), \quad (\text{A14})$$

where

$$f(y) = \left[\frac{e^{-y^2}}{\sqrt{\pi}[1 + \text{erf}(y)]} + y \right]^{-1} \quad (\text{A15})$$

is the scaling function of the scaling parameter

$$y = \frac{2\alpha - 1}{\sqrt{t}}. \quad (\text{A16})$$

- [1] *Frustrated Spin Systems*, edited by H. T. Diep (World Scientific, Singapore, 2013).
- [2] *Introduction to Frustrated Magnetism. Materials, Experiments, Theory*, edited by C. Lacroix, P. Mendels, and F. Mila (Springer-Verlag, Berlin, 2011).
- [3] *Quantum Magnetism*, Lecture Notes in Physics Vol. 645, edited by U. Schollwöck, J. Richter, D. J. J. Farnell, and R. F. Bishop (Springer-Verlag, Berlin, 2004).
- [4] D. Sen, B. S. Shastry, R. E. Walstedt, and R. Cava, *Phys. Rev. B* **53**, 6401 (1996).
- [5] T. Nakamura and K. Kubo, *Phys. Rev. B* **53**, 6393 (1996).
- [6] S. A. Blundell and M. D. Nuner-Reguerio, *Eur. Phys. J. B* **31**, 453 (2003).
- [7] O. Derzhko, J. Richter, and M. Maksymenko, *Int. J. Mod. Phys. B* **29**, 1530007 (2015).
- [8] M. E. Zhitomirsky and H. Tsunetsugu, *Phys. Rev. B* **70**, 100403(R) (2004); *Prog. Theor. Phys. Suppl.* **160**, 361 (2005).
- [9] J. Schulenburg, A. Honecker, J. Schnack, J. Richter, and H. J. Schmidt, *Phys. Rev. Lett.* **88**, 167207 (2002).
- [10] O. Derzhko and J. Richter, *Phys. Rev. B* **70**, 104415 (2004).
- [11] T. Tonegawa and M. Kaburagi, *J. Magn. Magn. Mater.* **272**, 898 (2004).
- [12] M. Kaburagi, T. Tonegawa, and M. Kang, *J. Appl. Phys.* **97**, 10B306 (2005).
- [13] V. Ya. Krivnov, D. V. Dmitriev, S. Nishimoto, S.-L. Drechsler, and J. Richter, *Phys. Rev. B* **90**, 014441 (2014).
- [14] D. V. Dmitriev and V. Ya. Krivnov, *Phys. Rev. B* **92**, 184422 (2015); *J. Phys.: Condens. Matter* **28**, 506002 (2016); **30**, 385803 (2018).
- [15] Y. Inagaki, Y. Narumi, K. Kindo, H. Kikuchi, T. Kamikawa, T. Kunimoto, S. Okubo, H. Ohta, T. Saito, H. Ohta, T. Saito, M. Azuma, H. Nojiri, M. Kaburagi, and T. Tonegawa, *J. Phys. Soc. Jpn.* **74**, 2831 (2005).
- [16] C. Ruiz-Perez, M. Hernandez-Molina, P. Lorenzo-Luis, F. Lloret, J. Cano, and M. Julve, *Inorg. Chem.* **39**, 3845 (2000).
- [17] R. Shirakami, H. Ueda, H. O. Jeschke, H. Nakano, S. Kobayashi, A. Matsuo, T. Sakai, N. Katayama, H. Sawa, K. Kindo, C. Michioka, and K. Yoshimura, *Phys. Rev. B* **100**, 174401 (2019).
- [18] A. Baniodeh, N. Magnani, Y. Lan, G. Buth, C. E. Anson, J. Richter, M. Affronte, J. Schnack, and A. K. Powell, *npj Quantum Mater.* **3**, 10 (2018).
- [19] J. Schnack, *Contemp. Phys.* **60**, 127 (2019).
- [20] D. V. Dmitriev, V. Ya. Krivnov, J. Richter, and J. Schnack, *Phys. Rev. B* **99**, 094410 (2019).
- [21] J. Richter and J. Schulenburg, *Eur. Phys. J. B* **73**, 117 (2010); <https://www-e.uni-magdeburg.de/jschulen/spin>.
- [22] J. Jaklic and P. Prelovsek, *Phys. Rev. B* **49**, 5065 (1994); *Adv. Phys.* **49**, 1 (2000).
- [23] J. Schnack and O. Wendland, *Eur. Phys. J. B* **78**, 535 (2010); J. Schnack, J. Schulenburg, and J. Richter, *Phys. Rev. B* **98**, 094423 (2018).
- [24] V. R. Chandra, D. Sen, N. B. Ivanov, and J. Richter, *Phys. Rev. B* **69**, 214406 (2004).
- [25] M. Blume, P. Heller, and N. A. Lurie, *Phys. Rev. B* **11**, 4483 (1975).
- [26] I. Harada and H. J. Mikeska, *Z. Phys. B: Condens. Matter* **72**, 391 (1988).
- [27] M. Takahashi, H. Nakamura, and S. Sachdev, *Phys. Rev. B* **54**, R744 (1996).
- [28] J. F. Marko and E. D. Siggia, *Macromolecules* **28**, 8759 (1995).
- [29] M. Takahashi, *Phys. Rev. Lett.* **58**, 168 (1987); *Phys. Rev. B* **36**, 3791 (1987).